KSCE Journal of Civil Engineering (2022) 26(2):650-660
DOI 10.1007/s12205-021-0660-2

pISSN 1226-7988, eISSN 1976-3808
www.springer.com/12205

Geotechnical Engineering

Hydraulic and Mechanical Coupling Analysis of Rough Fracture Network under Normal Stress and Shear Stress

Tianjiao Yang[a], **Shuhong Wang**[a], **Pengyu Wang**[a], **and Ze Zhang**[a]

[a]*College of Resources and Civil Engineering, Northeastern University, Shenyang 110819, China*

ARTICLE HISTORY

Received 15 April 2021
Revised 7 August 2021
Accepted 31 August 2021
Published Online 27 October 2021

KEYWORDS

Normal stress
Shear stress
Hydraulic and mechanical coupling
Fracture intersection point
Rough fracture

ABSTRACT

The hydraulic and mechanical coupling characteristics of fracture networks under normal stress and shear stress were studied in this paper. The hydraulic and mechanical coupling model of the fracture network comprehensively considers the normal stress, shear stress, seepage pressure and roughness characteristics. Based on the boundary conditions and reasonable assumptions, COMSOL Multiphysics software was used to develop the hydraulic and mechanical coupling finite element model of the fracture network with different intersection points under normal stress and shear stress, focusing on the study of the effect of normal stress and shear stress on the fracture permeability. The degree of permeability change caused by the normal stress and shear stress is different. The shear stress has a significant influence on the fracture permeability, and when the normal stress is low, the relationship between the fracture permeability and shear stress can be described by a linear relationship. Then, the influence of the number of intersection points in the fracture network on the average fracture width, average water pressure, average seepage velocity and seepage passage of the fractured rock mass was analyzed. The number of intersections in the fracture network has little influence on the average fracture gap width and average water pressure but has a great influence on the flow velocity. The analysis in this paper is very helpful to understand the seepage characteristics in rough fractures under normal stress and shear stress.

1. Introduction

Compared with intact rock masses, the seepage characteristics of fractured rock masses are determined mainly by structural surfaces (Ma et al., 2015; Yin et al., 2021), and show complex flow characteristics such as strong medium inhomogeneity (Zou et al., 2018; Shao et al., 2020; Zhang et al., 2020). Under stress, dilatancy leads to an increase in fracture openings (Esaki et al., 1999; Li et al., 2008; Javadi et al., 2014), while normal stress will lead to a decrease in fracture openings (Durham and Bonner, 1994; Zhang and Nemcik, 2013; Son, 2020); therefore, it is very important to carry out research on the seepage characteristics of fractures (fracture networks) under stress (Zhao et al., 2011; Huenges et al., 2013; Yin et al., 2017). At the beginning of the 20th century, Terzaghi clearly put forward the principle of effective stress to establish a one-dimensional consolidation model of homogeneous saturated soil, which is the basic theory and primal model of coupled seepage and stress in soil media (Terzaghi, 1943). In the middle of the 20th century, Biot applied Terzaghi's theory to the analysis of a three-dimensional consolidation model of saturated soils, and gave some classic formulas, which laid the foundation for theoretical research on groundwater fluid-solid coupling (Biot, 1941). Therefore, based on Biot theory, the change in hydraulic conductivity caused by deformation has received more attention (Pham et al., 2016), and it has been coupled to a fully poroelastic model to evaluate seepage characteristics (Mahyari and Selvadurai, 1998; Selvadurai, 2004; Selvadurai and Shirazi, 2010; Zhu and Wei, 2011; Guo et al., 2012; Zhu et al., 2014).

For fractured rock masses, early researchers focused on studying the influence of normal stress on the hydraulic and mechanical coupling characteristics of fractured rock masses. There are three methods: 1) We directly establish the empirical fitting relationship between permeability and stress based on the results of seepage tests (Gale, 1982). Although these research results can characterize the basic hydraulic and mechanical coupling characteristics of fractured rock masses, they are all purely empirical formulas

CORRESPONDENCE Shuhong Wang shwang@mail.neu.edu.cn College of Resources and Civil Engineering, Northeastern University, Shenyang 110819, China

based on test data fitting, and cannot explain some special hydraulic characteristics of fractures, such as the fracture permeability not being zero under high pressure. 2) The coupling relationship between permeability and stress is explained by using experimental or numerical simulation methods through the establishment of a conceptual model. Tsang and Witherspoon proposed a bulge-cave combination model (Tsang and Witherspoon, 1981), in which the cave and bulge in the fracture face control the deformation and seepage characteristics of the fracture respectively, which can represent the feature of low permeability of the feature under the action of high stress. Therefore, this method can explain the shortcomings of the first method. However, due to its large theoretical assumptions, the method does not match the actual features, which also makes the hydraulic and mechanical coupling model that is obtained biased. 3) According to the deformation and seepage laws of the fracture surface, the theoretical model of permeability and stress is established indirectly, and the single fracture hydraulic and mechanical coupling model is established through experiments and theoretical derivation (Yeo, 2001; Souley et al., 2015), which has become the single fracture hydraulic and mechanical coupling research hotspot. Early research scholars believed that the fracture permeability is completely determined by the square of the fracture hydraulic opening (Zimmerman and Bodvarsson, 1996; Zhang and Nemcik, 2013), which makes a minor change in the crack hydraulic opening cause a significant change in the permeability. Generally, the surface of natural cracks has rough characteristics, and the existence of rough characteristics makes the seepage law of fractures inconsistent with the cubic law (Lemarchand et al., 2010; Ju et al., 2013; Develi and Babadagli, 2015; Pyrak-Nolte and Nolte, 2016), and the roughness characteristics will change under the action of external stress. Therefore, it is particularly important to analyze the effects of stress and geometric characteristics on fracture permeability (Javadi et al., 2014; Chen et al., 2015; Zou et al., 2015; Liu et al., 2016; Ma et al., 2021). Wang proposed and analyzed a new model of seepage mechanism characteristics coupled with confining pressure to investigate the effect of confining pressure on the seepage mechanism characteristics (Wang et al., 2021b) and carried out experiments on shale samples containing three types of fractures: a single short fracture, a single long fracture, and symmetrical short fractures using a confining pressure pump to determine the seepage characteristics (Wang et al., 2021a). The above material shows that the third method has a sound theoretical basis and considers a number of factors affecting the mechanical properties of the fracture, which makes it more applicable than the first and second methods. In summary, the effects of stress and crack roughness are the two key factors that must be considered in the current study of fracture hydraulic and mechanical coupling (Ni et al., 2014).

In the past two decades, due to engineering needs and the development of computers, experiments and numerical models have been used to study the hydraulic conductivity of fractures under shear stress and complex stress (Nguyen and Selvadurai, 1998; Olsson and Barton, 2001; He and Zhuang, 2019; Lei et al., 2021). Compared with the research progress on the hydraulic and mechanical coupling characteristics of the normal stress of a single fracture, the shear and seepage coupling characteristics of a single fracture have been less studied, mainly because it is difficult to guarantee the sealing of the permeating fluid during the shear test (Jiang et al., 2004; Auradou et al., 2005; Koyama et al., 2012). At present, some scholars characterize the influence of the fracture dilatancy effect on the seepage characteristics by measuring the normal displacement of the fracture surface during the shear process (Rong et al., 2016; Vogler et al., 2016; Gui et al., 2017). The evolution of the geometric characteristics of the fracture is the mechanism by which the roughness affects the shear and seepage coupling characteristics, and it is also the focus of the current research. Similar studies can also be found in other literature (Koyama et al., 2004; Xiong et al., 2011). In terms of simulation, Xie used the COMSOL multiphysics simulation program to solve the Navier-Stokes formula to calculate and analyze the seepage features of a single crack during shear displacements, and obtained the equivalent hydraulic gap width, mechanical gap width, and the law of the change in volume velocity with shear displacement. At the same time, the distribution characteristics of fluid volume velocity in fractures under different shear directions and different shear displacements are analyzed (Xie et al., 2015). Min established a theoretical model of fracture network rock masses that considers the nonlinear normal deformation and dilatancy effects of cracks through the Universal Distinct Element Code (UDEC) and carried out a series of numerical simulation studies on the permeability characteristics under different stress states and discussed the influence of fracture normal closure on the equivalent permeability coefficient (Min et al., 2004).

From the above overall analysis, the current research on hydraulic and mechanical coupling characteristics of fractures has the following shortcomings: 1) Due to the dynamic characteristics of the shear process, it is difficult to establish a theoretical model, so the hydraulic and mechanical coupling model under the joint action of normal stress and shear stress is seldom studied. 2) Although these experiments and model analyses provide basic knowledge about the change in seepage characteristics of a single rough fracture under stress, the actual engineering rock mass is composed of multiple fractures, and limited experimental conditions cannot fully analyze this problem. In the numerical simulation, even though some models consider the impact of the discrete fracture network on the fluid flow characteristics, these models have not considered the impact of the number of fracture intersection points on the seepage characteristics for specific analysis. Based on the Patton model and Plesha theoretical model, the Plesha model including hydraulic behavior was extended. By assuming that the change in the fracture width is connected to the plastic work of the shear stress of the fracture surface, the relationship between the permeability and mechanical width of the fracture is deduced, and then the model of the influence of rough single fracture on fracture permeability under compressive and shear stresses is obtained (Nguyen and Selvadurai, 1998). This paper applies this model to the numerical simulation of the rough

fracture network model with different numbers of intersections to analyze the seepage characteristics in the rough fractured rock mass. This paper presents a hydraulic and mechanical coupling model of a fractured rock mass that comprehensively considers the normal stress, shear stress, seepage pressure and roughness characteristics. A numerical calculation method is used to calculate and analyze the hydraulic and mechanical seepage characteristics of fractured rock masses under normal and shear stresses. In this study, through the calculation of fracture network models with different numbers of intersection points, the focus is on the comparison of the impact of normal stress and shear stress acting on the rock mass on the fracture permeability, and the influence of the number of fracture intersection points on the average fracture width, average water pressure, average seepage velocity and seepage channel.

2. Governing Equations for Mechanical and Hydraulic Coupling Behavior in a Fracture

Constitutive laws for fractured rock masses should be able to reproduce the basic mechanical properties of real fractures, such as dilation under shear stress. Among these properties, Nguyen and Selvadurai promoted the model of Plesha (Bandis et al., 1981) to contain hydraulic characteristics (Nguyen and Selvadurai, 1998). The fracture can experience dilation during shear stress, which leads to an initial increase in permeability. In the development of a coupled mechanical and hydraulic behavior model we use the constitutive governing equation.

2.1 Elastoplastic Modeling of the Mechanical Behavior

Bandis et al. (1981) experimentally observed that u_{peak}, the shear displacement corresponding to the peak value of shear stress τ_{peak} is applied with equal normal stress and can be considered independent of the normal stress. Assuming linear elastic behavior of the fracture up to the peak shear stress, we can obtain, the elastic shear stiffness k_s as follows:

$$k_s = \frac{|\tau_{peak}|}{u_{peak}} = \frac{\sigma \tan\left(JRCLog_{10}\left(JCS/\sigma\right)+\phi\right)}{\left(L/500\right)/\left(JRC/L\right)^{0.33}}, \tag{1}$$

where τ_{peak} is the peak shear stress, u_{peak} is the peak shear displacement, σ is the normal stress, JRC is the roughness coefficient of the structural surface, JCS is the uniaxial compressive strength of rock, L is the size length, and ϕ is the friction angle. The coefficients JRC (dimensionless) and JCS (MPa) and the friction angle ϕ can easily be estimated from two tests (Jaeger, 1971; Barton and Choubey, 1977): the tilt test and the Schmidt hammer test.

The parameters JRC and JCS are both scale-dependent. Bandis et al. proposed empirical relationships as follows (Bandis et al., 1981):

$$JRC = JRC_0\left(\frac{L}{L_0}\right)^{-0.02JRC_0}, \quad JCS = JCS_0\left(\frac{L}{L_0}\right)^{-0.02JRC_0}, \tag{2}$$

where JRC_0 and JCS_0 are laboratory-scale values, for joints with normal size L_0 = 100 mm and JRC and JCS are values for larger samples of size L.

The remaining parameter required for the model established by Plesha is the normal stiffness k_n. This parameter can be obtained by compression tests on fractured rock samples. The most comprehensive experimental investigations on the normal closure behavior of joints under applied normal stresses are due to Bandis et al., Bandis et al. proposed the hyperbolic relationship as follows (Bandis et al., 1981):

$$\sigma = k_{ni}\frac{v}{1-v/v_m}, \tag{3}$$

where k_{ni} is the normal stiffness when the normal stress is zero, v is the normal deformation of the fracture, and v_m is the maximum closure of the fracture.

The normal stiffness is then

$$k_n = \frac{d\sigma}{dv} = k_{ni}\left(1-\frac{\sigma}{v_m k_{ni}+\sigma}\right)^{-2}. \tag{4}$$

The parameters k_{ni} and v_m that enter Eq. (4) are best obtained by compression tests on fractured rock samples.

2.2 Hydraulic Behavior

The parallel plate model is usually used to calculate the fracture permeability k as follows (Kling et al., 2017; Medici et al., 2019):

$$k = e_h^{\,2}/12, \tag{5}$$

where e_h is the hydraulic aperture of the fracture.

Because naturally formed fractures are different from the ideal parallel plate models, the value of the fracture hydraulic aperture is not the same as its mechanical aperture. Witherspoon et al. established a linear relationship between the hydraulic aperture and the mechanical aperture (Witherspoon et al., 1979):

$$e_h = e_{h0} + f\Delta e_m, \tag{6}$$

where e_{h0} is the initial hydraulic aperture, Δe_m is the change in mechanical aperture because of the combined effects of normal and shear stresses as discussed in the above section, and f is a proportionality factor. Benjelloun experimentally verified the validity of Eq. (6), given that f changes between 0.5 and 1. This variable comes from the roughness of the fracture surfaces. A factor f = 1 applies to the limiting ideal case of parallel smooth plates; this situation prevails only when the joint is relatively open, with apertures of on order of mm. In the majority of situations, f < 1. The geometry of the flow path has an important influence on f. In rectilinear laminar flow, f is generally close to 0.8 and in radial flow, f is close to 0.5 (Nguyen and Selvadurai, 1998).

To simulate the effect of gouge production on the joint permeability, we assume that this effect is connected with the total plastic work because of shear stress. Adopting the form of the relation proposed by Plesha (Bandis et al., 1981), we assume that the factor f in Eq. (7) has a connection with the plastic work

produced by the shear forces according to the equation as follows:

$$f = f_0 \exp\left(- \int_0^{W^p} c_f dW^p \right), \tag{7}$$

where c_f is a gouge production factor. It is very likely that the plus parameters f_0 and c_f introduced in this section can have empirical connections with JRC, JCS and σ. A detailed experimental program will be needed to arrive at specific correlations. Plesha (Bandis et al., 1981) assumes that the plastic work is produced by the shear stress:

$$W^p = \int \tau du_1^p , \tag{8}$$

where $du_1 = du$ is the relative fracture shear displacement.

3. Simulation of Coupled Mechanical and Hydraulic Behavior of Rough Fracture Network

Although large-scale indoor model tests can better simulate and discuss the permeability characteristics under stress, it is relatively difficult to carry out large-scale experimental research due to the complex test operations and heavy workload. Compared with physical model tests, numerical simulation has been widely used in the research and discussion of related problems in the field of underground engineering seepage due to its convenient calculation, high repeatability, and low cost.

In this paper, to study the influence of normal stress, shear stress and the different number of fractured intersection points on the permeability characteristics, the analysis is divided into different working conditions, as shown in Table 1. The research

Table 1. Different Control Variables

The number of fracture intersection points N	Normal stress σ (kPa)	Shear stress τ (kPa)
Model 1: $N = 0$	2.5 – 10	0.2 – 0.8
Model 2: $N = 1$	2.5 – 10	0.2 – 0.8
Model 3: $N = 3$	2.5 – 10	0.2 – 0.8
Model 4: $N = 5$	2.5 – 10	0.2 – 0.8

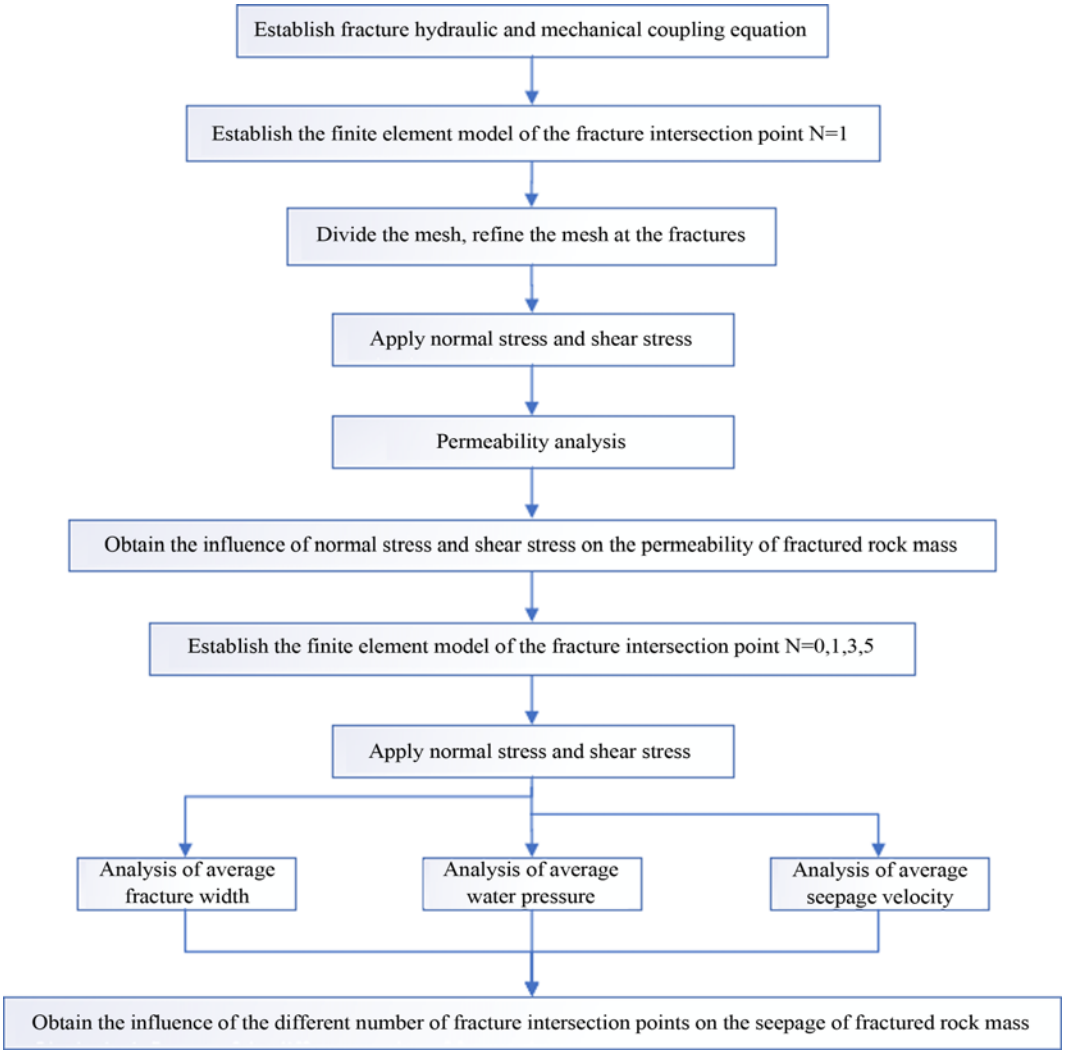

Fig. 1. Flowchart of Seepage of Fractured Rock Mass Analysis

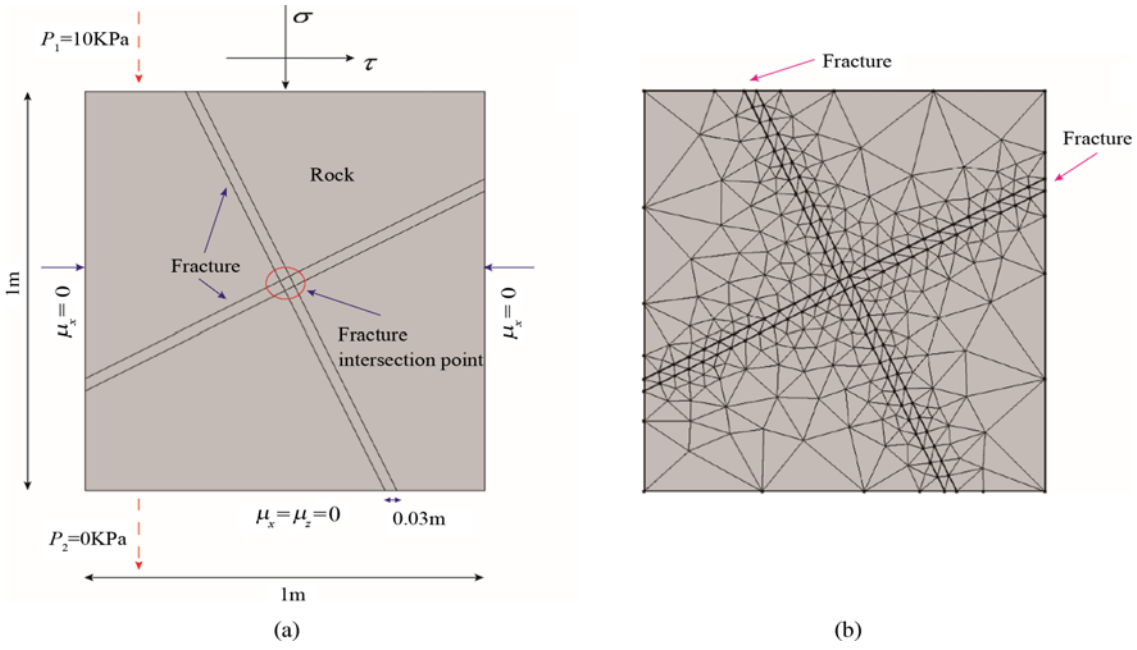

Fig. 2. Hydraulic and Mechanical Coupling Model of Fracture Intersection Point $N = 1$ under Normal and Shear Stress: (a) The Two-Dimensional Model, (b) The Finite Element Mesh

process of this paper is shown in Fig. 1.

The basic assumptions adopted in this paper when establishing the model are as follows:

1. The rock matrix is a homogeneous and isotropic linear elastic medium;
2. No fracture propagation occurs in the fracture matrix during the infiltration process;
3. Ignore the compressibility of fluid and the thermal effect of fluid flowing in fractures;
4. The density and dynamic viscosity coefficient of the fluid remain unchanged.

Figure 2(a) shows the hydraulic and mechanical coupling model of fracture intersection point $N = 1$ under normal stress and shear stress. In this model, the size of the model is 1 m × 1 m, and the boundary conditions and initial conditions of the model are as follows: the left, right and lower boundaries of the model are all displacement constraints, the normal stress is applied vertically to the upper boundary of the model, and the shear stress is applied horizontally to the upper boundary of the model. The fluid with a pressure of is injected vertically from the upper boundary of the model, and the water pressure P_1 at the lower boundary is P_2. The finite element mesh was generated using COMSOL Multiphysics software. A free triangular grid is used in the modeling process. The predefined element size is set as an adaptive mesh feature, and grid refinement near the fractures ensures the accuracy of the simulation. The resulting grid has 3519 elements, and 3,270 degrees of freedom and is shown in Fig. 2(b).

Table 2 lists the parameters of the hydraulic and mechanical coupling model of the fractured rock mass used in this study (Nguyen and Selvadurai, 1998).

Figure 3 demonstrates the variation in fracture permeability

Table 2. Model Calculation Physical Parameters

Parameter	Value	Units
ρ	3,070	kg/m^3
μ	0.25	1
k_{ni}	2E9	Pa/m
E	2.2	GPa
c	0.01	Pa · s
φ	37	rad
P_1	5	kPa
P_2	0	kPa
JRC	9	1
JCS	28	MPa
eh_0	0.03	m
k_0	7.5E-5	m^2

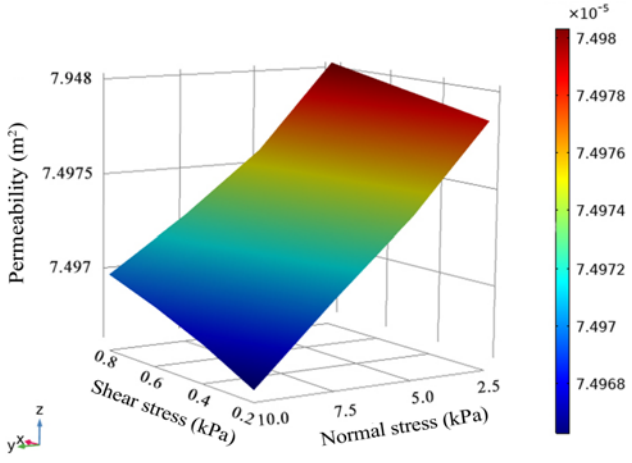

Fig. 3. Permeability Changes under Normal Stress and Shear Stress

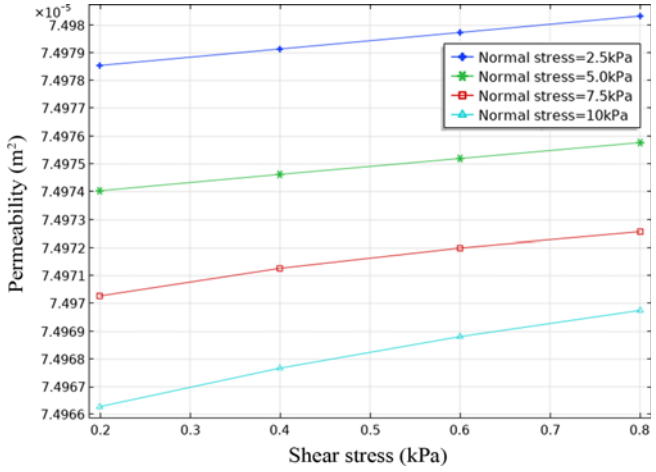

Fig. 4. $k_f - \tau$ Curve under Different Normal Stresses

with normal stress and shear stress loading. When the shear stress is 0.2 kPa, the difference in permeability reduction is 1E-7 m^2 as the normal stress increases. When the shear stress is 0.8 kPa, the difference in permeability reduction is 8E-8 m^2 as the normal stress increases. The normal stress clearly has a certain influence on the permeability of the fracture, and when the shear stress is constant, the permeability of the fracture decreases with increasing normal stress. At the same time, when the normal stress is low, the permeability changes greatly as the normal stress increases, and the permeability is sensitive to changes in the normal stress; when the normal stress reaches 6 kPa, the change in the permeability shows a decreasing trend, and the permeability is less sensitive to changes in the normal stress due to the decrease in fracture aperture caused by the increase in normal stress. However, comparing the effects of changes in normal and shear stresses acting on rock blocks on permeability, shear stress has a greater impact on permeability, so shear stress cannot be ignored when analyzing the permeability of fractured rock masses.

Figure 4 demonstrates the variation in fracture permeability with shear stress under different normal stresses. When the normal stress is 5 kPa, the difference in permeability is 1.8E-9 m^2 as the shear stress increases. When the normal stress is 10 kPa, the permeability difference is 3.6E-9 m^2 as the shear stress increases. It shows that when the normal stress is constant, the shear stress has a greater impact on the permeability of the fracture. The permeability increases with increasing shear stress, and when the normal stress is low, the permeability-shear stress curve has a better linear relationship. At the same time, the larger the normal stress, the steeper the slope of the $k_f - \tau$ curve. When the normal stress is different, the shear stress has a different effect on the permeability, and the influence of shear stress on permeability increases with increasing normal stress.

To study the seepage characteristics of the fracture network under stress, this paper also calculates and analyzes the model of the different numbers of fracture intersection points N. The size of the calculation model is 1 m × 1 m. The calculation model with different numbers of fracture intersection points N is shown

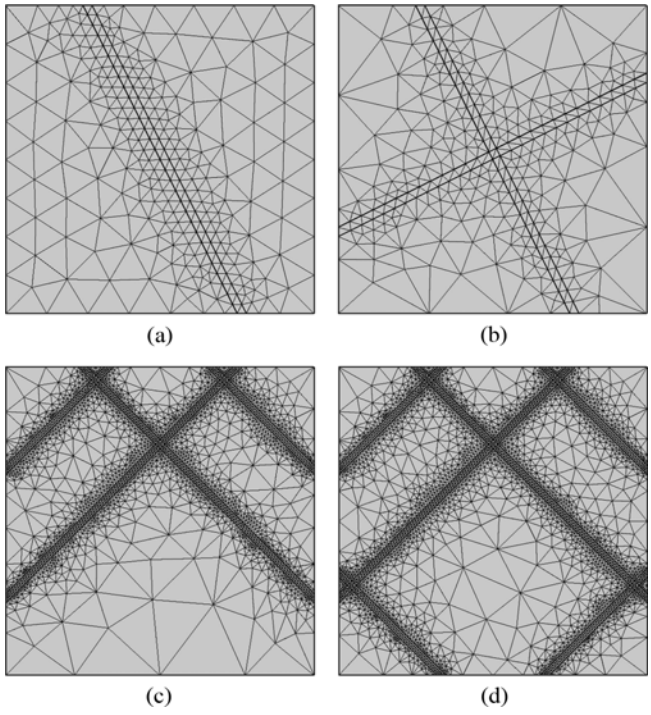

Fig. 5. Calculation Model and Meshing of Different Fracture Intersection Points: (a) $N = 0$, (b) $N = 1$, (c) $N = 3$, (d) $N = 5$

in Fig. 5. In the calculation process, the model parameters, boundary conditions and initial conditions are the same as the fracture intersection $N = 1$ model mentioned above.

In states of $\sigma = 5$ kPa and $\tau = 0.4$ kPa, the distribution characteristics of the average fracture width, average water pressure, average seepage velocity and seepage channels in the calculation model of the fractured rock mass with different numbers of fracture intersection points are shown in Figs. 6, 7 and 8.

Figure 6 shows that the fractures are all in a compressed state, and the fracture width is smaller than the initial fracture width (0.03 m). Since the fractures in the model with $N = 3$ and $N = 5$ fracture intersection points are bilaterally symmetrical, the distribution characteristics of the average fracture width are basically bilaterally symmetrical. When the number of fracture intersection points is different, the average fracture widths are all the largest on the lower side (0.02999 m), that is, the lower side of the changed fracture width is the smallest (1E-5 m), and the variation amplitude is the smallest. On the whole, the number of fracture intersections has little effect on the average crack width. When the number of fracture intersection points is 0, the maximum and minimum difference between the average fracture width is 6E-5 m. When the number of crack intersection points is 5, the maximum and minimum difference between the average fracture widths is 3E-5 m, which shows that the greater the number of fracture intersection points is, the smaller the influence on the average fracture width.

Figure 7 shows that the average water pressure of fractures in the model with the number of fracture intersection points $N = 3$ and $N = 5$ basically presenting a bilateral symmetrical structure

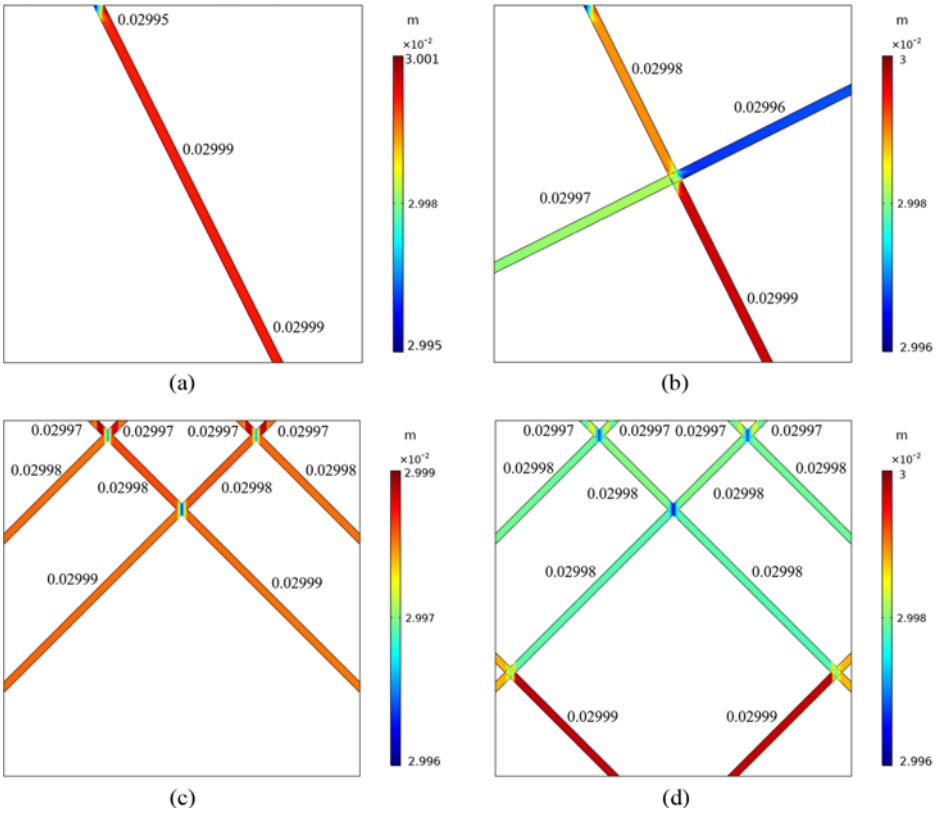

Fig. 6. Distribution Characteristics of the Average Fracture Width(m) of Models with Different Numbers of Fracture Intersection Points: (a) $N = 0$, (b) $N = 1$, (c) $N = 3$, (d) $N = 5$

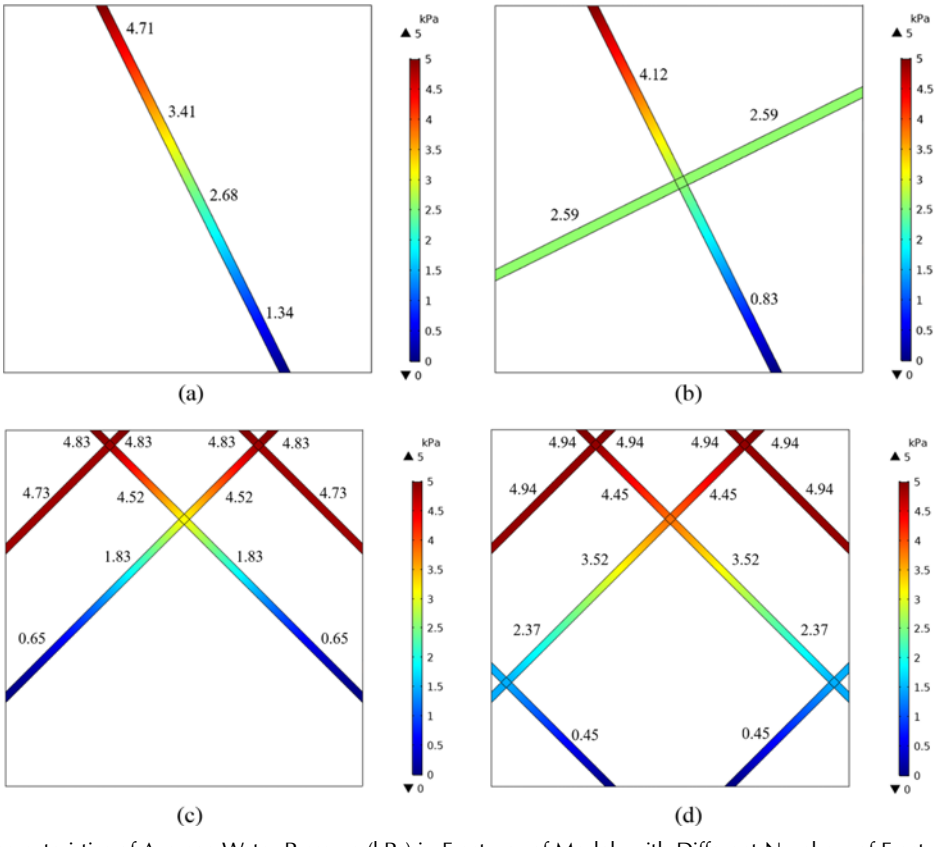

Fig. 7. Distribution Characteristics of Average Water Pressure (kPa) in Fractures of Models with Different Numbers of Fracture Intersection Points: (a) $N = 0$, (b) $N = 1$, (c) $N = 3$, (d) $N = 5$

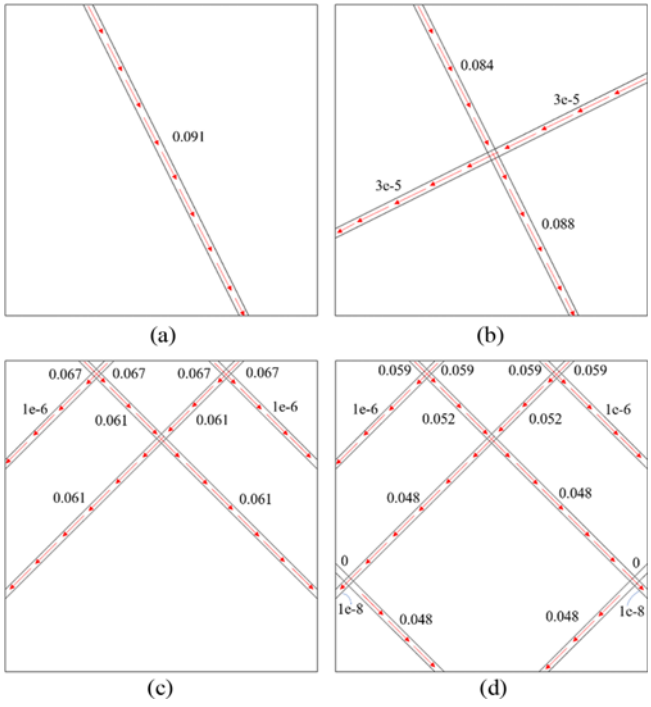

Fig. 8. Distribution Characteristics of the Average Seepage Velocity (m/s) and the Seepage Channel in Fractures of Models with Different Numbers of Fracture Intersection Points: (a) N = 0, (b) N = 1, (c) N = 3, (d) N = 5

distribution. On the whole, due to the upper and lower sides of the model acting on the water pressures of P_1 and P_2, the water pressure in the fracture network in the steady state shows a gradual decreasing trend from top to bottom. When the number of fracture intersection points is 0, 1, 3, and 5, the average water pressure in the fracture under the steady state of the models is 1.34 kPa, 0.83 kPa, 0.65 kPa, and 0.35 kPa, respectively. The greater the number of fracture intersection points is, the smaller the water pressure of fractures near the bottom of the model. Due to the difference in the number of fracture intersection points, the water pressure of fractures changes significantly, but the characteristics of the water pressure change with the number of intersections not showing obvious rules.

Since the connected rough fracture network in the fractured rock mass is the channel for fluid migration, the distribution characteristics of the seepage channel and the average velocity in the model with different numbers of intersection points of the fracture network are obviously different, as shown in Fig. 8. When the number of fracture intersection points is 0, there is only one seepage channel (shown by the red arrow) connecting the upper and lower boundaries in the model. At this time, the fracture has roughly the same fluid velocity (0.091 m/s). When the number of fracture intersection points is 1, 3 and 5, there are multiple complex seepage channels in the fracture network, and the seepage velocity in the fracture network is not the same in the steady state. When the number of fracture intersection points is 3 and 5, the average flow velocity in the fracture seepage channel in the steady state basically remains symmetric because this type of fracture network is symmetrical, which is similar to the distribution characteristics of the fracture width in Fig. 6.

Figure 8 also shows that the overall average flow velocities on the lower side of the model under different numbers of fracture network intersection points are 0.091 m/s ($N = 0$), 0.088 m/s ($N = 1$), 0.061 m/s ($N = 3$), and 0.048 m/s ($N = 5$). With the increase in the number of fracture intersection points, the seepage channels in the fracture network gradually become denser and more complex, and the average flow velocity at the outlet of the model gradually decreases because each branch of the intersecting fracture is composed of a single facture. When the inlet and outlet pressures of the fracture water flow are the same, the flow at the end of the fracture is redistributed at the intersection to form different boundary angles, and the water flow is affected by different degrees of resistance, which leads to energy loss, thereby reducing the flow velocity. From the intersection along the direction of each fracture, the generation of vortices gradually decreases the flow rate of the water flow. Compared with $N = 0$, when $N = 5$, the average flow velocity at the lower water outlet of the model is reduced by approximately 1.896 times. When the number of intersection points increases from $N = 0$ to $N = 1$, since the bottom of the model has the same number of fractured water outlets, the reduction of the average flow velocity at the model outlet is relatively small.

4. Conclusions

This paper mainly uses numerical calculation methods to calculate and analyze the seepage characteristics of rock masses with different fracture network intersection points under normal stress and shear stress. The focus is on the comparison of the impact of normal stress and shear stress acting on the rock mass on the fracture permeability and the influence of the number of fracture intersection points on the average fracture width, average water pressure, average seepage velocity and seepage channel. Specifically, the findings offer four important conclusions.

1. This paper comprehensively considers factors such as normal stress, shear stress, seepage pressure and roughness characteristics, and extends the calculation model of a single fracture to the hydraulic and mechanical coupling model with the different number of fracture intersection points under normal stress and shear stress, which solves the problem that it is difficult to control the shear stress and the number of fractures in the experiment to analyze the seepage characteristics of the fractured rock mass. This paper shows that shear stress has a great influence on fracture permeability when comparing the influence of the changes of normal stress and shear stress on permeability.
2. When the normal stress is constant, the shear stress has a significant effect on the permeability of the fracture, and the permeability of the fracture increases with increasing shear stress. When the normal stress changes, the influence of the shear stress on the permeability increases due to the increase in the normal stress. When the normal stress is

low, the relationship between fracture permeability and shear stress can be described by a linear relationship.

3. The number of fracture intersection points has an effect on the average fracture width and average water pressure of the fracture. When the number of fracture intersection points is different, the average fracture width on the lower side is the largest (0.02999 m), and the fracture water pressure shows a gradual decreasing trend from the upper to the lower side of the models. With the increase in the number of fracture intersection points, the influence on the average fracture width is smaller, and the influence on the fracture water pressure is larger. In general, the number of fracture intersection points has little influence on the average fracture width and average water pressure.
4. Since the connected fracture network in the fractured rock mass is the channel for fluid migration, with the increase in the number of fracture intersection points, the model has only one seepage channel connecting the upper and lower boundaries and increases to multiple complicated seepage channels. The water flow is affected by different degrees of resistance, leading to energy loss, thus reducing the flow velocity. Moreover, the seepage velocity in the fracture network under the stable state is also different. Compared with $N = 0$, when $N = 5$, the average flow velocity at the lower water outlet of the model is reduced by approximately 1.896 times. In general, the number of intersection points of the fracture network has a greater impact on the flow velocity.

Acknowledgments

This work was conducted with supports from the National Natural Science Foundation of China (Grant Nos.U1602232 and 51474050), Key science and technology projects of Liaoning Province, China (2019JH2-10100035), the Fundamental Research Funds for the Central Universities (N170108029; N180701005).

ORCID

Tianjiao Yang https://orcid.org/0000-0002-4302-2539
Shuhong Wang https://orcid.org/0000-0003-1737-2815
Pengyu Wang https://orcid.org/0000-0001-8024-9858
Ze Zhang https://orcid.org/0000-0001-7609-6588

References

Auradou H, Drazer G, Hulin JP, Koplik J (2005) Permeability anisotropy induced by the shear displacement of rough fracture walls. *Water Resources Research* 41(9):1-10, DOI: 10.1029/2005wr003938

Bandis S, Lumsden AC, Barton NR (1981) Experimental studies of scale effects on the shear behaviour of rock joints. *International Journal of Rock Mechanics and Mining Sciences & Geomechanics Abstracts* 18(1):1-21, DOI: 10.1016/0148-9062(81)90262-X

Barton NR, Choubey V (1977) The shear strength of rock joints in theory and practice. *Rock Mechanics and Rock Engineering* 10(1):1-54, DOI: 10.1007/BF01261801

Biot MA (1941) General theory of three-dimensional consolidation. *Journal of Applied Physics* 12(2):155-164, DOI: 10.1063/1.1712886

Chen YF, Zhou JQ, Hu SH, Hu R, Zhou CB (2015) Evaluation of Forchheimer equation coefficients for non-Darcy flow in deformable rough-walled fractures. *Journal of Hydrology* 529:993-1006, DOI: 10.1016/j.jhydrol.2015.09.021

Develi K, Babadagli T (2015) Experimental and visual analysis of single-phase flow through rough fracture replicas. *International Journal of Rock Mechanics and Mining Sciences* 73:139-155, DOI: 10.1016/j.ijrmms.2014.11.002

Durham WB, Bonner BP (1994) Self-propping and fluid flow in slightly offset joints at high effective pressures. *Journal of Geophysical Research Atmospheres* 99(B5):9391-9399, DOI: 10.1016/0148-9062(95)90081-0

Esaki T, Du S, Mitani Y, Ikusada K, Jing L (1999) Development of a shear-flow test apparatus and determination of coupled properties for a single rock joint. *International Journal of Rock Mechanics & Mining Sciences* 36(5):641-650, DOI: 10.1016/S0148-9062(99)00044-3

Gale JE (1982) The effects of fracture type (induced versus natural) on the stress-fracture closure-fracture permeability relationships. The 23rd US symposium on rock mechanics (USRMS), August 25-27, Berkeley, CA, USA

Gui Y, Xia CC, Ding WQ (2017) A new method for 3D modeling of joint surface degradation and void space evolution under normal and shear loads. *Rock Mechanics and Rock Engineering* 50(10):2827-2836, DOI: 10.1007/s00603-017-1242-y

Guo H, Yuan L, Shen BT, Qu QD, Xue JH (2012) Mining-induced strata stress changes, fractures and gas flow dynamics in multi-seam longwall mining. *International Journal of Rock Mechanics & Mining Sciences* 54:129-139, DOI: 10.1016/j.ijrmms.2012.05.023

He B, Zhuang XY (2019) Coupled discrete crack and porous media model for hydraulic fractures using the XFEM. *KSCE Journal of Civil Engineering* 23(3):1017-1027, DOI: 10.1007/s12205-019-0449-8

Huenges E, Kohl T, Kolditz O, Bremer J, Vienken T (2013) Geothermal energy systems: Research perspective for domestic energy provision. *Environmental Earth Sciences* 70(8):3927-3933, DOI: 10.1007/s12665-013-2881-2

Jaeger JC (1971) Friction of rocks and stability of rock slopes. *Geotechnique* 21:97-134, DOI: 10.1680/geot.1971.21.2.97

Javadi M, Sharifzadeh M, Shahriar K, Mitani Y (2014) Critical Reynolds number for nonlinear flow through rough-walled fractures: The role of shear processes. *Water Resources Research* 50(2):1789-1804, DOI: 10.1002/2013WR014610

Jiang Y, Xiao J, Tanabashi Y, Mizokami T (2004) Development of an automated servo-controlled direct shear apparatus applying a constant normal stiffness condition. *International Journal of Rock Mechanics and Mining Sciences* 41(2):275-86, DOI: 10.1016/j.ijrmms.2003.08.004

Ju Y, Zhang Q, Yang Y, Xie HP, Gao F, Wang HJ (2013) An experimental investigation on the mechanism of fluid flow through single rough fracture of rock. *Science China Technological Sciences* 56(8):2070-2080, DOI: 10.1007/s11431-013-5274-6

Kling T, Schwarz JO, Wendler F, Enzmann F, Blum P (2017) Fracture flow due to hydrothermally induced quartz growth. *Advances in Water Resources* 107:93-107, DOI: 10.1016/j.advwatres.2017.06.011

Koyama T, Fardin N, Jing L (2004) Shear induced anisotropy and heterogeneity of fluid flow in a single rock fracture by translational and rotary shear displacements - A numerical study. *International Journal of Rock Mechanics and Mining Sciences* 41(3):426-436,

DOI: 10.1016/j.ijrmms.2003.12.026
Koyama T, Li B, Jiang Y, Jing L (2012) Coupled shear-flow tests for rock fractures with visualization of the fluid flow and their numerical simulations. *International Journal of Geotechnical Engineering* 2(3):215-227, DOI: 10.3328/IJGE.2008.02.03.215-227
Lei QH, Doonechaly NG, Tsang CF (2021) Modelling fluid injection-induced fracture activation, damage growth, seismicity occurrence and connectivity change in naturally fractured rocks. *International Journal of Rock Mechanics and Mining Sciences*138:104598, DOI: 10.1016/j.ijrmms.2020.104598
Lemarchand E, Davy CA, Dormieux L, Skoczylas F (2010) Tortuosity effects in coupled advective transport and mechanical properties of fractured geomaterials. *Transport in Porous Media* 84(1):1-19, DOI: 10.1007/s11242-009-9481-3
Li B, Jiang Y, Koyama T, Jing L, Tanabashi Y (2008) Experimental study of the hydro-mechanical behavior of rock joints using a parallel-plate model containing contact areas and artificial fractures. *International Journal of Rock Mechanics & Mining Sciences* 45(3): 362-375, DOI: 10.1016/j.ijrmms.2007.06.004
Liu R, Li B, Jiang YJ (2016) Critical hydraulic gradient for nonlinear flow through rock fracture networks: The roles of aperture, surface roughness, and number of intersections. *Advances in Water Resources* 88:53-65, DOI: 10.1016/j.advwatres.2015.12.002
Ma GW, Jing HW, Yin Q (2015) Experimental study on mechanical properties of sandstone specimens containing a single hole after high-temperature exposure. *Géotechnique Letters* 5:43-48, DOI: 10.1680/geolett.14.00121
Ma HC, Wang JP, Qian, JZ, Tan XH, Ma L (2021) Two-dimensional SPH analysis of seepage with water injection process for different crack morphologies. *KSCE Journal of Civil Engineering* 25(5): 1909-1917, DOI: 10.1007/s12205-021-1202-7
Mahyari AT, Selvadurai APS (1998) Enhanced consolidation in brittle geomaterials susceptible to damage. *Mechanics of Cohesive-Frictional Materials* 3(3):291-303, DOI: 10.1002/(SICI)1099-1484(199807)3:33.0.CO;2-K
Medici G, West LJ, Banwart SA (2019) Groundwater flow velocities in a fractured carbonate aquifer-type: Implications for contaminant transport. *Journal of Contaminant Hydrology* 222:1-16, DOI: 10.1016/j.jconhyd.2019.02.001
Min KB, Rutqvist J, Tsang CF, Jing L (2004) Stress-dependent permeability of fractured rock masses: A numerical study. *International Journal of Rock Mechanics & Mining Sciences* 41(7):1191-1210, DOI: 10.1016/j.ijrmms.2004.05.005
Nguyen TS, Selvadurai APS (1998) A model for coupled mechanical and hydraulic behaviour of a rock joint. *International Journal for Numerical and Analytical Methods in Geomechanics* 22(1):29-48, DOI: 10.1002/(SICI)1096-9853(199801)22:1<29::AID-NAG907>3.0.CO;2-N
Ni X, Yang JB, Shao JF (2014) Study on the hydromechanical behavior of single fracture under normal stresses. *KSCE Journal of Civil Engineering* 18(9):1641-1649, DOI: 10.1007/s12205-014-0490-6
Olsson R, Barton N (2001) An improved model for hydromechanical coupling during shearing of rock joints. *International Journal of Rock Mechanics and Mining Sciences* 38(3):317-329, DOI: 10.1016/S1365-1609(00)00079-4
Pham K, Choi HJ, Lee D, Kim K, Choi H (2016) Effect of Biot's coefficient and fluid properties on isothermal H-M coupled consolidation analysis of porous media. *KSCE Journal of Civil Engineering* 20(6):2355-2364, DOI: 10.1007/s12205-015-1463-0
Pyrak-Nolte LJ, Nolte DD (2016) Approaching a universal scaling relationship between fracture stiffness and fluid flow. *Nature Communications* 7:10663, DOI: 10.1038/ncomms10663
Rong G, Yang J, Cheng L, Zhou CB (2016) Laboratory investigation of nonlinear flow characteristics in rough fractures during shear process. *Journal of Hydrology, ElsevierB.V* 541:1385-1394, DOI: 10.1016/j.jhydrol.2016.08.043
Selvadurai APS (2004) Stationary damage modelling of poroelastic contact. *International Journal of Solids and Structures* 41(8):2043-2064, DOI: 10.1016/j.ijsolstr.2003.08.023
Selvadurai APS, Shirazi A (2010) An elliptical disc anchor in a damage-susceptible poroelastic medium. *International Journal for Numerical Methods in Engineering* 63:2017-2039, DOI: 10.1002/nme.1354
Shao JF, Zhang Q, Wu XT, Lei Y, Wang ZY (2020) Investigation on the water flow evolution in a filled fracture under seepage-induced erosion. *Water* 12(11):3188, DOI: 3188.10.3390/w12113188
Son M (2020) Shear strength of rock joints and its estimation. *KSCE Journal of Civil Engineering* 24(10):2931-2938, DOI: 10.1007/s12205-020-0296-7
Souley M, Lopez P, Boulon M, Thoraval A (2015) Experimental hydromechanical characterization and numerical modelling of a fractured and porous sandstone. *Rock Mechanics and Rock Engineering* 48(3):1143-1161, DOI: 10.1007/s00603-014-0626-5
Terzaghi KT (1943) Theoretical soil mechanics. Wiley and Sons, New York, NY, USA, DOI: 10.1002/9780470172766
Tsang YW, Witherspoon PA (1981) Hydromechanical behavior of a formable rock fracture subject to normal stress. *Journal of Geophysical Research* 86(B10):9287-9298, DOI: 10.1029/JB086iB10p09287
Vogler D, Amann F, Bayer P, Elsworth D (2016) Permeability evolution in natural fractures subject to cyclic loading and gouge formation. *Rock Mechanics and Rock Engineering* 49(9):3463-3479, DOI: 10.1007/s00603-016-1022-0
Wang JP, Ma HC, Feng PC, Zhang Q, Wu D (2021a) An experimental study on seepage within shale fractures due to confining pressure and temperature. *KSCE Journal of Civil Engineering* 25(9):3596-3604, DOI: 10.1007/s12205-021-5025-3
Wang JP, Ma HC, Qian JZ, Feng PC, Ma L (2021b) Experimental and theoretical study on the seepage mechanism characteristics coupling with confining pressure. *Engineering Geology* 291(4):106224, DOI: 10.1016/j.enggeo.2021.106224
Witherspoon PA, Amick CH, Gale JE, Iwai K (1979) Observations of a potential size effect in experimental determination of the hydraulic properties of fractures. *Water Resources Research* 15:1142-1146, DOI: 10.1029/WR015i005p01142
Xie LZ, Gao C, Ren L, Li CB (2015) Numerical investigation of geometrical and hydraulic properties in a single rock fracture during shear displacement with the Navier–Stokes equations. *Environmental Earth Sciences* 73(11):7061-7074, DOI: 10.1007/s12665-015-4256-3
Xiong XB, Li B, Jiang YJ, Koyama T, Zhang CH (2011) Experimental and numerical study of the geometrical and hydraulic characteristics of a single rock fracture during shear. *International Journal of Rock Mechanics and Mining Sciences* 48(8):1292-1302, DOI: 10.1016/B978-0-12-408083-6.00022-2
Yeo IW (2001) Effect of contact obstacles on fluid flow in rock fractures. *Geosciences Journal* 5(2):139-143, DOI: 10.1007/BF02910418
Yin Q, Jing HW, Zhu TT (2017) Experimental study on mechanical properties and cracking behavior of pre-cracked sandstone specimens under uniaxial compression. *Indian Geotechnical Journal* 47:265-279, DOI: 10.1007/s40098-016-0210-x
Yin Q, Jing HW, Zhu TT, Wu L, Yu L (2021) Spatiotemporal evolution characteristics of fluid flow through large-scale 3D rock mass containing

filling joints: An experimental and numerical study. *Geofluids* 1-23, DOI: 10.1155/2021/8883861

Zhang XB, Chen HH, Yao C, Yang JH, Zhou CB (2020) Seepage characteristics of triaxial compression-induced fractured rocks under varying confining pressures. *International Journal of Geomechanics* 20(9):04020160, DOI: 10.1061/(ASCE)GM.1943-5622.0001796

Zhang ZY, Nemcik J (2013) Fluid flow regimes and nonlinear flow characteristics in deformable rock fractures. *Journal of Hydrology* 477(1):139-151, DOI: 10.1016/j.jhydrol.2012.11.024

Zhao Z, Jing L, Neretnieks I, Moreno L (2011) Numerical modeling of stress effects on solute transport in fractured rocks. *Computers & Geotechnics* 38(2):113-126, DOI: 10.1016/j.compgeo.2010.10.001

Zhu WC, Wei CH (2011) Numerical simulation on mining-induced water inrushes related to geologic structures using a damage based hydromechanical model. *Environmental Earth Sciences* 62(1):43-45, DOI: 10.1007/s12665-010-0494-6

Zhu B, Wu Q, Yang JW, Cui T (2014) Study of pore pressure change during mining and its application on water inrush prevention: A numerical simulation case in Zhaogezhuang coalmine, China. *Environmental Earth Sciences* 71(5):2115-2132, DOI: 10.1007/s12665-013-2616-4

Zimmerman RW, Bodvarsson GS (1996) Hydraulic conductivity of rock fractures. *Transport in Porous Media* 23(1):1-30, DOI: 10.1007/BF00145263

Zou LC, Jing LR, Cvetkovic V (2015) Roughness decomposition and nonlinear fluid flow in a single rock fracture. *International Journal of Rock Mechanics and Mining Sciences* 75:102-118, DOI: 10.1016/j.ijrmms.2015.01.016

Zou LF, Xu WY, Meng GT, Ning Y, Wang HL (2018) Permeability anisotropy of columnar jointed rock masses. *KSCE Journal of Civil Engineering* 22(10):3802-3809, DOI: 10.1007/s12205-018-0123-6